

Article

Effect of Nb on the Microstructure and Mechanical Properties of Ti_2Cu Intermetallic through the First-Principle Calculations and Experimental Investigation

Jialin Cheng ^{1,2,*}, Yeling Yun ¹, Jingjing Wang ¹, Jiaxin Rui ¹, Shun Wang ^{3,*} and Yulei Du ^{4,*}¹ School of Materials Science and Engineering, Nanjing Institute of Technology, Nanjing 211167, China; yunyeling1994@163.com (Y.Y.); wangjingjing142857@163.com (J.W.); NJIT_Rjx@163.com (J.R.)² Jiangsu Key Laboratory of Advanced Structural Materials and Application Technology, Nanjing 211167, China³ School of Materials Science and Engineering, Henan University of Technology, Zhengzhou 450001, China⁴ School of Mechanical Engineering, Nanjing University of Science and Technology, Nanjing 210094, China

* Correspondence: chengjialin@njit.edu.cn (J.C.); shun_wang@haut.edu.cn (S.W.); yldu_njust@njust.edu.cn (Y.D.); Tel.: +86-025-8611-8278 (J.C.); +86-0371-6775-8729 (S.W.); +86-025-8431-5446 (Y.D.)

Received: 17 March 2020; Accepted: 22 April 2020; Published: 23 April 2020



Abstract: Through the first-principle calculations based on density functional theory and experimental investigation, the structural stability elastic properties and mechanical properties of Ti_2Cu and $Ti_{18}Cu_5Nb_1$ intermetallics were studied. The first-principle calculations showed that the ratio of bulk modulus to shear modulus (B/G) and Poisson's ratio (ν) of Ti_2Cu and $Ti_{18}Cu_5Nb_1$ intermetallics were 2.03, 0.288, and 2.22, 0.304, respectively, indicating that the two intermetallics were ductile. This was confirmed by the compression tests, which showed that the plastic strain of both intermetallics was beyond 25%. In addition, the yield strength increased from the 416 to 710 MPa with the addition of Nb. The increase in strength is the result of three factors, namely covalent bond tendency, fine grain strengthening, and solid solution strengthening. This finding gives clues to design novel intermetallics with excellent mechanical properties by first-principle calculations and alloying.

Keywords: intermetallic alloys and compounds; microstructure; deformation and fracture; simulation and modeling

1. Introduction

Intermetallics are distinctive compounds with strong interatomic binding force, high melting point, good creep resistance, and oxidation resistance as well as excellent electrical, magnetic, and acoustic properties [1–5]. Many efforts have been spent to develop the Ti-Al [6–9], Ni-Al [10–12], and Fe-Al [13–15] intermetallics, which have been used as high temperature structural materials, superconducting materials, and corrosion resistant coatings. However, most intermetallics exhibit a macroscopically brittle failure at ambient temperature, which severely limits their wide applications.

Until now, many researchers have been devoted to improving the ductility of intermetallics including alloying [16–19] and synthesizing methods [20–25]. Some alloying elements such as B, Cr, and V have been applied to enhance the room temperature plasticity of the Fe-Al, Ni-Al, and Ti-Al intermetallics. However, the toughening mechanism of microalloying is still under discussion, and the design and preparation of intermetallics with intrinsic toughness is still a challenge. Recently, some researchers [26–28] have reported that the toughness of intermetallics can be predicted through

the ratio of bulk modulus to shear modulus (B/G) and Poisson's ratio (ν). These parameters can be calculated by the elastic properties and electronic structures of intermetallics using first-principles based on the density functional theory (DFT). Therefore, the first-principle calculations were applied to investigate the elastic properties and electronic structures of intermetallics such as Ti-Al, Fe-Al, and Cu-Li. However, there have been few studies and reports on the Ti_2Cu intermetallic, which has been widely used to enhance the mechanical properties of the Ti-based alloys. Therefore, it is important to explore the electron structure, stability, and mechanical properties of the Ti_2Cu intermetallic.

In this paper, we systematically explored the elastic properties and electronic structures of Ti_2Cu and intermetallics using the first-principle full-potential linearized augmented plane-wave (FP-LAPW) method. The stability and mechanical properties of the Ti_2Cu intermetallic were predicted theoretically and verified by experimental investigation. Moreover, the effects of Nb alloying on the elastic properties, electronic structures, and mechanical properties of the Ti_2Cu intermetallic were also studied.

2. Computational and Experimental Methods

The first-principle calculations were performed using FP-LAPW based on the DFT. The WIEN2k calculation software package was used to calculate the exchange correlation energy using the generalized gradient approximation (GGA) [29]. The cut-off parameter $R_{mt}K_{max}$ was fixed at -7.0 Ry. The muffin-tin sphere radii (R_{mt}) used for Ti, Cu, and Nb were 2.4, 2.5, and 2.5 a.u., respectively. The self-consistent calculations were considered to be converged when the total energy was within 10^{-5} Ry/unit cell. The Brillouin zone integrations were performed with 1000 k -points.

Alloy button ingots with nominal compositions of $Ti_{66.7}Cu_{33.3}$ and $Ti_{61.7}Cu_{33}Nb_5$ (at. %) were prepared by arc-melting the mixtures of Ti, Cu, and Nb metal chips with purities higher than 99.5 wt. % under a Ti-gettered argon atmosphere. The alloy ingots were completely re-melted, and cast into a copper mold to form rod-shaped samples with 7 mm diameters by gravity casting. The structure of the samples was analyzed by using a Rigaku D/max 2038 x-ray diffractometer (Rigaku Corporation, Tokyo, Japan) (XRD) with Cu $K\alpha$ radiation operated at 40 KV and 300 mA. Measurements were performed by step scanning 2θ from 20 to 90 with a 0.02° step size, and a count time of 1 s per step was used. Microstructural observations were carried out using optical microscopy (OM). Cylindrical specimens with a 3 mm diameter and 6 mm length were used for the compression tests, and ends of the specimens were mechanically polished. Uniaxial compression tests were conducted on an Instron-8801 testing machine at room temperature using an engineering strain rate of $5 \times 10^{-4} \text{ s}^{-1}$. At least three samples for mechanical testing were measured to ensure that the results were reproducible and statistically meaningful. The fracture surfaces of the deformed samples were examined using an FEI XL-30 scanning electron microscopy (SEM, FEI Company, Hillsboro, OR, USA) operated at 15 kV.

3. Results and Discussion

The Ti_2Cu intermetallic is a tetragonal structure and its spatial group is I4/mmm (NO.139). A Ti_2Cu intermetallic cell contains two Cu atoms and four Ti atoms. Cu and Ti atoms occupy 2A (0, 0, 0) and 4E (0, 0, u) positions, respectively, as shown in Figure 1a. To investigate the effects of Nb alloying on the structural, electronic, and elastic properties of the Ti_2Cu intermetallic, one Ti atom was replaced by a Nb atom in a 2×2 supercell of Ti_2Cu , as shown in Figure 1b. The molecular formula was $Ti_{15}Cu_8Nb$.

The full structural optimizations of Ti_2Cu and $Ti_{15}Cu_8Nb$ were performed both over the lattice parameters and the atomic positions. The calculated values of the structural parameters a , c ; atomic coordinate u ; and interatomic distances d with available experimental data for Ti_2Cu and $Ti_{15}Cu_8Nb$ are summarized in Table 1. It can be found that the calculated structural parameters were very consistent with the experimental ones and the relative error was less than 1%. The results indicate that the present computational method is reliable. There was a slight increase in the nearest atomic distance d_{Nb-Ti1} , d_{Nb-Ti2} , d_{Nb-Cu1} of the Nb atom for $Ti_{15}Cu_8Nb$ in comparison with Ti_2Cu , which can be deduced from the fact that Nb has a larger atomic radius than Ti.

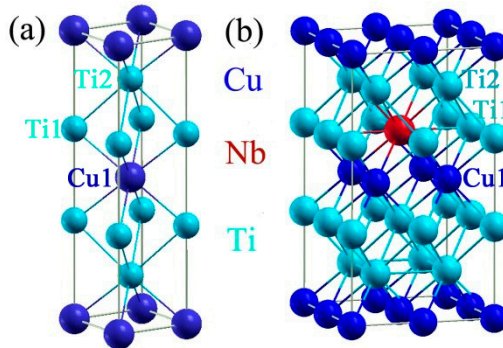


Figure 1. Crystal structures of Ti₂Cu (a) and Ti₁₅Cu₈Nb (b).

Table 1. Calculate the structural parameters $a(\text{\AA})$, $b(\text{\AA})$, $c(\text{\AA})$, c/a , u , and interatomic distances $d(\text{\AA})$ for Ti₂Cu and Ti₁₅Cu₈Nb with the experimental data from [30].

Alloy	a	b	c	c/a	u	$d_{\text{Ti1-Ti1}}/d_{\text{Nb-Ti1}}$	$d_{\text{Ti1-Ti2}}/d_{\text{Nb-Ti2}}$	$d_{\text{Ti1-Cu1}}/d_{\text{Nb-Cu1}}$
Ti ₂ Cu	2.936	2.936	10.770	3.6675	0.338	2.936/-	2.809/-	2.713/-
Experimental Values [30]	2.943	2.943	10.784	3.6643	0.341	-	-	-
Ti ₁₅ Cu ₈ Nb	5.881	5.881	10.784	-	-	-/2.941	-/2.836	-/2.743

The elastic constants are important parameters for engineering applications. Six independent elastic constants (C_{ij} , namely C_{11} , C_{12} , C_{33} , C_{44} , C_{13} , and C_{66}) for the tetragonal Ti₂Cu and Ti₁₅Cu₈Nb intermetallics were evaluated by means of calculating the stress tensors on the different deformations applied to the equilibrium lattice. Thus, the dependence between the resulting energy change and deformation was determined with the full relaxation of atomic positions. The calculated elastic constants are listed in Table 2. For the tetragonal crystal, its mechanical stability requires that its independent C_{ij} should satisfy Born's criteria [31]:

$$\left\{ \begin{array}{l} C_{ii} > 0, i = 1, 3, 4, 6 \\ C_{11} - C_{12} > 0 \\ C_{11} + C_{33} - 2C_{13} > 0 \\ 2(C_{11} + C_{12}) + C_{33} + 4C_{13} > 0 \end{array} \right. \quad (1)$$

Table 2. Calculated elastic constants C_{ij} of the Ti₂Cu and Ti₁₅Cu₈Nb intermetallics.

Alloy	C_{11} (GPa)	C_{12} (GPa)	C_{33} (GPa)	C_{44} (GPa)	C_{66} (GPa)	C_{13} (GPa)
Ti ₂ Cu	215	84	186	95	52	106
Ti ₁₅ Cu ₈ Nb	220	96	186	97	51	116

From Table 2, we can see that these criteria were all satisfied, which indicates that the Ti₂Cu and Ti₁₅Cu₈Nb intermetallics are mechanically stable.

According to the elastic constants, the bulk modulus B , shear modulus G , Young's modulus E and Poisson's ratio ν can also be calculated using the Voigt-Reusse-Hill (VRH) method and the following equations [32]:

$$B_V = (2C_{11} + 2C_{12} + C_{33} + 4C_{13})/9 \quad (2)$$

$$G_V = (M + 3C_{11} - 3C_{12} + 12C_{44} + 6C_{66})/30 \quad (3)$$

$$B_R = C^2/M \quad (4)$$

$$G_R = 15/\left[\frac{18B_v}{C^2} + \frac{6}{C_{11} - C_{12}} + \frac{6}{C_{44}} + \frac{3}{C_{66}}\right] \quad (5)$$

$$C^2 = (C_{11} + C_{12})C_{33} - 2C_{13}^2 \quad (6)$$

$$M = C_{11} + C_{12} + 2C_{33} - 4C_{13} \quad (7)$$

$$B_H = (B_R + B_V)/2 \quad (8)$$

$$G_H = (G_R + G_V)/2 \quad (9)$$

$$E = 9BG/(3B + G) \quad (10)$$

$$\nu = (3B - E)/6B = (3B - 2G)/(6B + 2G) \quad (11)$$

The elastic modulus and Poisson's ratio were calculated and listed in Table 3. According to the previous report [26–28,33,34], the values of B/G and ν can determine the brittle/ductile behavior of solid materials. The critical values of B/G and ν were 1.75 and 0.26, beyond which the solid materials exhibited a ductile behavior. For the Ti_2Cu and $Ti_{15}Cu_8Nb$ intermetallics, the values of B/G and ν were 2.03 and 0.288, and 2.22 and 0.304, respectively. Therefore, it is reasonable to speculate that the Ti_2Cu and $Ti_{15}Cu_8Nb$ intermetallics have excellent ductility.

Table 3. B , G , E , and ν of the Ti_2Cu intermetallic.

Alloy	B (GPa)	G (GPa)	E (GPa)	B/G	ν
Ti_2Cu	134	66	149	2.03	0.288
$Ti_{15}Cu_8Nb$	142	64	167	2.22	0.304

To ascertain the inherent influencing mechanism of Nb on the bonding interactions of Ti_2Cu , the total and partial densities of states (DOS) of Ti_2Cu and $Ti_{15}Cu_8Nb$ were plotted in Figure 2. For the Ti_2Cu intermetallic (see Figure 2a), the states in the energy range of −5 to 0 eV were mainly occupied by the Cu-3d and Ti-3d states with less contribution from the 4s and 3p states of Cu and Ti atoms. Five major peaks at −3.6 eV, −3.1 eV, −1.8 eV, −1.2 eV, and −0.8 eV mainly originated from the coupling between Cu-3d and Ti-3d electrons, exhibiting a covalent bond feature. The states in the vicinity of the Fermi level (E_F) were mainly contributed by the Ti-3d state. The non-zero DOS value at E_F indicates the metallic electrical conductivity. The bonding characteristics of DOS for $Ti_{15}Cu_8Nb$ were similar to that for Ti_2Cu , as shown in Figure 3b. Whereas the coupling effects between Nb-4d, Cu-3d, and Ti-3d were significantly increased, resulting from the higher DOS values of Nb-4d than Ti-3d. These strong coupling effects were further confirmed by the planar projection of the total charge density of the (110) plane for Ti_2Cu and $Ti_{15}Cu_8Nb$, as shown in Figure 3. According to the charge density map, the charge density of Ti and Cu near Nb redistributed, and the Nb-Cu and Nb-Ti bonds were enhanced by the overlapping of the electron charge.

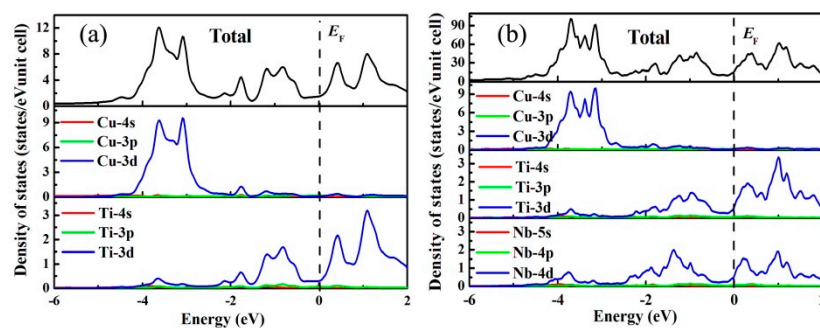


Figure 2. Total and partial density of the state curves of alloys (a) Ti_2Cu and (b) $Ti_{15}Cu_8Nb$.

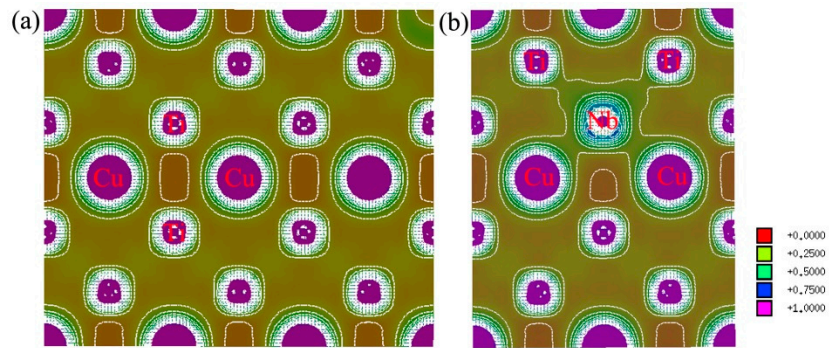


Figure 3. The planar projection of total charge density of the (110) plane from $0 \text{ e}/\text{\AA}^3$ to $1 \text{ e}/\text{\AA}^3$ for (a) Ti_2Cu and (b) $\text{Ti}_{15}\text{Cu}_8\text{Nb}$.

To obtain the effective atomic charge, Bader charge analysis was also carried out [35]. For Ti_2Cu , about 0.569 electrons transferred from one Ti atom to Cu atoms. The Ti–Cu bonds exhibited the ionic bonding property. After the Ti atoms were replaced by more electronegative atoms of Nb, one Nb atom gained about 0.612 electrons from neighbor Ti atoms. The calculated Bader charges of Cu1, Ti1, and Ti2 for $\text{Ti}_{15}\text{Cu}_8\text{Nb}$ were -1.078 , $+0.739$, and $0.740 \left|e\right|$, respectively. It can be seen that Cu gained fewer electrons from Ti atoms, implying a weaker ionic bonding feature of $\text{Ti}_{15}\text{Cu}_8\text{Nb}$ than Ti_2Cu . Consequently, an optimizing effect in improving the strength and toughness of Ti_2Cu may be produced due to the bonding interaction tendency from ionicity to covalency.

To investigate the mechanical properties of the intermetallics, we prepared the samples with nominal compositions of $\text{Ti}_{66.7}\text{Cu}_{33.3}$ and $\text{Ti}_{61.7}\text{Cu}_{33}\text{Nb}_5$ (at. %), which corresponded to the Ti_2Cu and $\text{Ti}_{15}\text{Cu}_8\text{Nb}$ intermetallics using copper mold casting. Figure 4 shows the microstructures and XRD patterns of the $\text{Ti}_{66.7}\text{Cu}_{33.3}$ and $\text{Ti}_{61.7}\text{Cu}_{33}\text{Nb}_5$ alloys. As shown, the two alloys showed typical lamellar structures composed of Ti_2Cu and TiCu phases. The volume fraction of the TiCu phase was about 5% for the two alloys. It is noteworthy that there was an obvious refining effect of the grain with the addition of Nb, where the lamellar spacing significantly decreased from 15 to 7 μm . This is because the slow diffusion of Nb restricts the growth rate of the crystals.

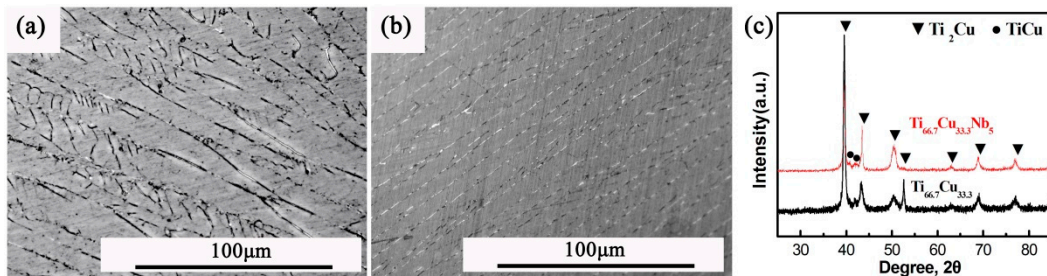


Figure 4. Microstructures of the $\text{Ti}_{66.7}\text{Cu}_{33.3}$ (a), $\text{Ti}_{61.7}\text{Cu}_{33}\text{Nb}_5$ (b) alloys and their x-ray diffraction (XRD) patterns (c).

Figure 5 shows the room temperature compressive stress–strain curves of the $\text{Ti}_{66.7}\text{Cu}_{33.3}$ and $\text{Ti}_{61.7}\text{Cu}_{33}\text{Nb}_5$ alloys. As shown, the yielding stress, ultimate compression stress, and plastic strain of the $\text{Ti}_{66.7}\text{Cu}_{33.3}$ alloy were 416 MPa, 1313 MPa, and 25.4%, respectively. This large plastic strain further confirms the ductility of the Ti_2Cu intermetallic predicted by first-principle calculations. Moreover, it is exciting to find that the yielding stress of the $\text{Ti}_{61.7}\text{Cu}_{33}\text{Nb}_5$ alloy significantly increased to 710 MPa without sacrificing the overall ductility. The result indicates that Nb alloying has a remarkable strengthening effect, which was also found in previous reports [36,37], but the strengthening mechanism is still controversial. In the present study, we believe that the increase in strength is the result of three factors. First, according to the results of first-principle calculations, the resonance and coupling

effects of electron clouds were increased due to the addition of Nb, and resulted in the enhancement of the covalent bond tendency, which is favorable to improve the alloy strength. Second, fine grain strengthening plays an important role because the lamellar spacing of $\text{Ti}_{61.7}\text{Cu}_{33.3}\text{Nb}_5$ was much lower than that of the Ti_2Cu alloy. In addition, the solid solution strengthening of Nb also significantly increased the strength of the alloy.

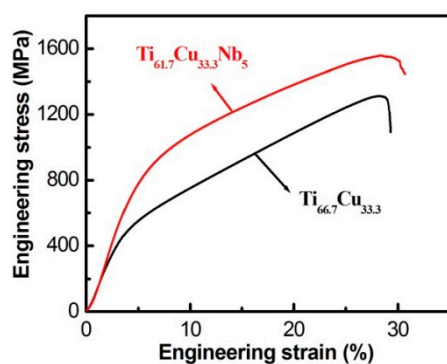


Figure 5. The compressive stress–strain curves of the $\text{Ti}_{66.7}\text{Cu}_{33.3}$ and $\text{Ti}_{61.7}\text{Cu}_{33.3}\text{Nb}_5$ alloys.

Figure 6 shows the fracture morphologies of two alloys. As shown, there were many microcracks (shown by white arrows) in different directions on the fracture surface of the two alloys, which was different from the shear fracture of the brittle materials. In addition, a large number of slip bands could be observed (shown by the black arrows) on the fracture surface and crack inside. These results indicate the ductility of the alloys. However, the origin of ductility in the present intermetallics is still unclear. Further studies should be carried out from the theoretical calculations and experimental research.

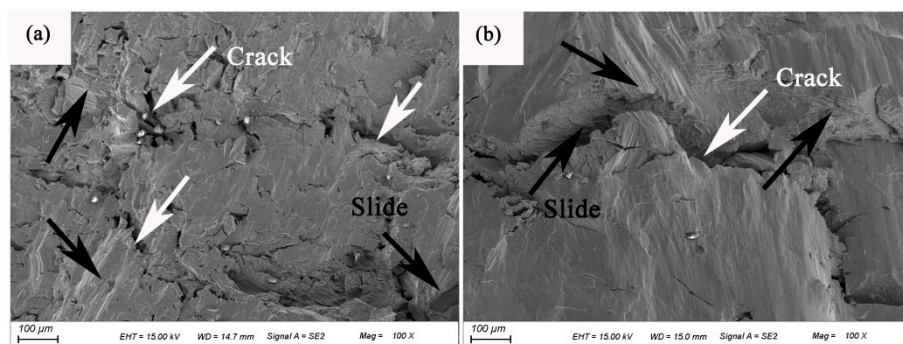


Figure 6. Scanning electron microscopy (SEM) micrographs of fracture surface for (a) $\text{Ti}_{66.7}\text{Cu}_{33.3}$ and (b) $\text{Ti}_{61.7}\text{Cu}_{33.3}\text{Nb}_5$.

4. Conclusions

In summary, the first-principle calculations were used to predict and explore the mechanical properties of Ti_2Cu and $\text{Ti}_{18}\text{Cu}_5\text{Nb}$ intermetallics. According to the first-principle calculations, the values of B/G and ν of the Ti_2Cu and $\text{Ti}_{18}\text{Cu}_5\text{Nb}$ intermetallics were 2.03 and 0.288, and 2.22 and 0.304, respectively, which were much larger than the critical values of 1.75 and 0.26, indicating that the two intermetallics were ductile. To investigate the mechanical properties of the intermetallics, we prepared the samples with nominal compositions of $\text{Ti}_{66.7}\text{Cu}_{33.3}$ and $\text{Ti}_{61.7}\text{Cu}_{33.3}\text{Nb}_5$ (at. %), that corresponded to the Ti_2Cu and $\text{Ti}_{15}\text{Cu}_8\text{Nb}$ intermetallics using copper mold casting. The compression tests showed that the plastic strain of both intermetallics was beyond 25%, confirming their ductility predicted by the first-principle calculations. It is noteworthy that the yielding stress significantly increased from 416 to 710 MPa with the addition of Nb. The strengthening mechanisms contributed to the three factors, namely, the covalent bond tendency, fine grain strengthening. And solid solution

strengthening. This finding gives clues as to the design of novel intermetallics with excellent mechanical properties by first-principle calculations and alloying.

Author Contributions: Conceptualization J.C., S.W. and Y.D.; methodology, Y.Y., J.W. and J.R.; software S.W. and Y.D.; writing J.C. and S.W.; funding acquisition J.C. and S.W. All authors have read and agreed to the published version of the manuscript.

Funding: This work was supported by the Excellent Youth Foundation of Jiangsu Scientific Committee (BK20180106), the Innovation Funds of Nanjing Institute of Technology (Grant No. CKJA201703), the Innovative Foundation Project for Students of Jiangsu Province (201811276024), the Fundamental Research Funds for the Henan Provincial Colleges and Universities (No. 2017QNJJH33), the Foundation of Henan Educational Committee (No. 19A430011), and the High Level Talent Foundation of Henan University of Technology (No. 2017BS002).

Conflicts of Interest: The authors declare no conflicts of interest.

References

- Ward-Close, C.M.; Minor, R.; Doorbar, P.J. Intermetallic-matrix composites—a review. *Intermetallics* **1996**, *4*, 217–229. [[CrossRef](#)]
- Liu, C.; George, E.P.; Maziasz, P.J.; Schneibel, J.H. Recent advances in B2 iron aluminide alloys: Deformation, fracture and alloy design. *Mater. Sci. Eng. A* **1998**, *258*, 84–98. [[CrossRef](#)]
- Stoloff, N.S.; Liu, C.T.; Deevi, S.C. Emerging applications of intermetallics. *Intermetallics* **2000**, *8*, 1313–1320. [[CrossRef](#)]
- Blaber, M.G.; Arnold, M.D.; Ford, M.J. A review of the optical properties of alloys and intermetallics for plasmonics. *J. Phys. Condens. Matter* **2010**, *22*, 143201. [[CrossRef](#)] [[PubMed](#)]
- Zamanzade, M.; Barnoush, A.; Motz, C. A review on the properties of iron aluminide intermetallics. *Crystals* **2016**, *6*, 10. [[CrossRef](#)]
- Wu, X. Review of alloy and process development of TiAl alloys. *Intermetallics* **2006**, *14*, 1114–1122. [[CrossRef](#)]
- Chen, G.; Peng, Y.B.; Zheng, G.; Qi, Z.X.; Wang, M.Z.; Yu, H.C.; Dong, C.L.; Liu, C.T. Polysynthetic twinned TiAl single crystals for high-temperature applications. *Nat. Mater.* **2016**, *15*, 876–881. [[CrossRef](#)]
- Han, J.; Li, X.; Dippenaar, R.; Liss, K.D.; Kawasaki, M. Microscopic plastic response in a bulk nano-structured TiAl intermetallic compound processed by high-pressure torsion. *Mater. Sci. Eng. A* **2018**, *714*, 84–92. [[CrossRef](#)]
- He, Y.; Liu, Z.; Zhou, G.; Wang, H.; Bai, C.G.; Rodney, D.; Appel, F.; Xu, D.S.; Yang, R. Dislocation dipole-induced strengthening in intermetallic TiAl. *Scripta Mater.* **2018**, *143*, 98–102. [[CrossRef](#)]
- Wei, L.; Zhao, Z. Fabrication of the lamellar NiAl nanochannel by selective phase dissolution of NiAl–Cr (Mo) eutectic alloy. *Corros. Sci.* **2018**, *138*, 142–145. [[CrossRef](#)]
- Wu, X.; Wang, C. Influence of alloying elements upon the theoretical tensile strength of Ni-based model superalloy: γ -Ni/ γ' -Ni₃Al multilayer. *Comput. Mater. Sci.* **2016**, *119*, 120–129. [[CrossRef](#)]
- Peng, J.; Fang, X.; Qu, Z.; Wang, J. Isothermal oxidation behavior of NiAl and NiAl-(Cr, Mo) eutectic alloys. *Corros. Sci.* **2019**, *151*, 27–34. [[CrossRef](#)]
- Wang, Y.; Vecchio, K.S. Microstructure evolution in Fe-based-aluminide metallic–intermetallic laminate (MIL) composites. *Mater. Sci. Eng. A* **2016**, *649*, 325–337. [[CrossRef](#)]
- Zamanzade, M.; Hasemann, G.; Motz, C.; Krüger, M.; Barnoush, A. Vacancy effects on the mechanical behavior of B2-FeAl intermetallics. *Mater. Sci. Eng. A* **2018**, *712*, 88–96. [[CrossRef](#)]
- Siemiaszko, D.; Kuzia, J. The influence of large particles of iron powder on the microstructure and properties of FeAl intermetallic phase. *Intermetallics* **2019**, *104*, 16–23. [[CrossRef](#)]
- Aoki, K.; Izumi, O. Improvement in room temperature ductility of the L1₂ type intermetallic compound Ni₃Al by boron addition. *J. Jpn. Inst. Met.* **1979**, *43*, 1190–1196. [[CrossRef](#)]
- Makamey, C.G.; Horton, J.A.; Liu, C.T. Effect on chromium on properties of Fe₃Al. *J. Mater. Res.* **1989**, *5*, 1156–1163. [[CrossRef](#)]
- Liu, C.; George, E.P.; Oliver, W.C. Grain-boundary fracture and boron effect in Ni₃Si alloys. *Intermetallics* **1996**, *4*, 77–83. [[CrossRef](#)]
- Hu, D. Effect on boron addition on the tensile ductility in lamellar TiAl alloys. *Intermetallics* **2002**, *10*, 851–858. [[CrossRef](#)]

20. Cahn, R.W. *Multiphase intermetallics, High-temperature Structural Materials*; Cahn, R.W., Evans, A.G., McLean, M., Eds.; Springer: Dordrecht, The Netherlands, 1996; pp. 79–91.
21. Chen, R.; Guo, J.; Yin, W.; Zhou, J. Superplasticity of a multiphase Ni-25Al-25Cr intermetallic alloy. *Scripta Mater.* **1999**, *40*, 209–215. [[CrossRef](#)]
22. Wang, Y.; Wang, H.; Liu, X.; Vecchio, K.S. Microstructure evolution in pure Ni and Invar-based Metallic-Intermetallic Laminate (MIL) composites. *Mater. Sci. Eng. A* **2017**, *682*, 454–465. [[CrossRef](#)]
23. Rohatgi, A.; Harach, D.J.; Vecchio, K.S.; Harvey, K.P. Resistance-curve and fracture behavior of Ti-Al₃Ti metallic-intermetallic laminate (MIL) composites. *Acta Mater.* **2003**, *51*, 2933–2957. [[CrossRef](#)]
24. Lu, Z.; Jiang, F.; Chang, Y.; Niu, Z.; Wang, Z.; Guo, C. Multi-phase intermetallic mixture structure effect on the ductility of Al₃Ti alloy. *Mater. Sci. Eng. A* **2018**, *721*, 274–285. [[CrossRef](#)]
25. Lu, Z.; Wei, N.; Li, P.; Guo, C.; Jiang, F. Microstructure and mechanical properties of intermetallic Al₃Ti alloy with residual aluminum. *Mater. Des.* **2016**, *110*, 466–474. [[CrossRef](#)]
26. Zhang, X.; Huang, W.; Ma, H.; Yu, H.; Jiang, W. First-principles prediction of the physical properties of ThM2Al20 (M= Ti, V, Cr) intermetallics. *Solid State Commun.* **2018**, *284–286*, 75–83. [[CrossRef](#)]
27. Yu, J.; Zhou, D.; Pu, C.; Tang, X.; Zhang, F. Prediction of stable Cu-Li binary intermetallics from first-principles calculations: Stoichiometries, crystal structures, and physical properties. *J. Alloys. Compd.* **2018**, *766*, 640–648. [[CrossRef](#)]
28. Xing, H.; Dong, A.; Huang, J.; Zhang, J.; Sun, B. Revisiting intrinsic brittleness and deformation behavior of B2 NiAl intermetallic compound: A first-principles study. *J Mater Sci Technol.* **2018**, *34*, 620–626. [[CrossRef](#)]
29. Blaha, P.; Schwarz, K.; Madsen, G.K.H.; Kvasnicka, D.; Luitz, J. WIEN2k; Vienna University of Technology: Vienna, Austria, 2001; ISBN 3-9501031-1-2.
30. Eremenko, V.N.; Buyanov, Y.I.; Prima, S.B. Phase diagram of the system Ti-Cu. *Sov. Powder. Metall. Met. Ceram.* **1966**, *5*, 494–502. [[CrossRef](#)]
31. Wu, Z.; Zhao, E.; Xiang, H.; Hao, X.; Liu, X.; Meng, J. Crystal structures and elastic properties of superhard IrN₂ and IrN₃ from first principles. *Phys. Rev. B* **2007**, *76*, 054115. [[CrossRef](#)]
32. Chen, S.; Sun, Y.; Duan, Y.; Huang, B.; Peng, M. Phase stability, structural and elastic properties of C15-type Laves transition-metal compounds MCo₂ from first-principles calculations. *J Alloy Comp.* **2015**, *630*, 202–208. [[CrossRef](#)]
33. Pugh, S.F. Relations between the elastic moduli and the plastic properties of polycrystalline pure metals. *Philos. Mag.* **1954**, *45*, 823–843. [[CrossRef](#)]
34. Wang, Z.; Gao, W.; Liu, Y.; Li, R.; Meng, F.; Song, J.; Qi, Y. A first principles investigation of W_{1-x}Mo_x (x=0-68.75 at.%) alloys: Structural, electronic, mechanical and thermal properties. *J. Alloys Compd.* **2020**, *829*, 154480. [[CrossRef](#)]
35. Bader, R.F.W. *Atom in Molecules: A Quantum Theory*; Oxford University Pres: Oxford, UK, 1990; p. 155.
36. Zhang, W.; Deevi, S.C.; Chen, G. On the origin of superior high strength of Ti-45Al-10Nb alloys. *Intermetallics* **2002**, *10*, 403–406. [[CrossRef](#)]
37. Paul, J.D.H.; Appel, F.; Wagner, R. The compression behaviour of niobium alloyed γ -titanium alumindies. *Acta Mater.* **1998**, *46*, 1075–1085. [[CrossRef](#)]



© 2020 by the authors. Licensee MDPI, Basel, Switzerland. This article is an open access article distributed under the terms and conditions of the Creative Commons Attribution (CC BY) license (<http://creativecommons.org/licenses/by/4.0/>).